First-principles study of the structural and elastic properties of zirconia

Giuseppe Fadda,[1,*] Luciano Colombo,[1,2,†] and Giovanni Zanzotto[3,‡]

[1]*Dipartimento di Fisica, Università degli Studi di Cagliari, Cittadella Universitaria, I-09042 Monserrato (CA), Italy*

[2]*Sardinian Laboratory for Computational Materials Science (SLACS), INFM-CNR, Cittadella Universitaria, I-09042 Monserrato (CA), Italy*

[3]*Dipartimento di Metodi e Modelli Matematici per le Scienze Applicate, Università degli Studi di Padova, Via Trieste, 63, I-35121 Padova (PD), Italy*

(Received 2 December 2008; published 2 June 2009)

Zirconia (ZrO_2) is a most important substance in materials science and technology due to its wide-ranging applications. Accordingly, there have been several investigations of its observed crystalline polymorphs. However, a systematic analysis of the elastic properties of the ZrO_2 structures is still lacking. In this paper the structural and elastic properties of the experimentally confirmed phases of zirconia are studied with density-functional theory. Comparisons are drawn among various methods of computing the elastic parameters as well as with existing experimental data and other theoretical investigations.

DOI: 10.1103/PhysRevB.79.214102 PACS number(s): 61.66.−f, 62.20.−x

I. INTRODUCTION

Zirconium dioxide ZrO_2 (zirconia) is a very interesting material as it combines excellent mechanical (high fracture toughness and bulk modulus), thermal (low thermal conductivity, extremely refractory), chemical (chemically inert, corrosion resistant), and dielectric (high dielectric constant) properties. There are consequently many technological applications of this substance, ranging from solid-oxide fuel-cell design to oxygen detection, from nuclear waste confinement to thermal barrier coating, from microelectronics to bone prosthetics in dentistry and orthopaedy (see for instance Refs. 1–8 and the references therein).

Zirconia exists under at least five crystalline phases with different symmetries[9,10] (see Fig. 1). The monoclinic $P2_1/c$ polymorph is the only one found at room conditions whereas the tetragonal $P4_2/nmc$ and the cubic $Fm\bar{3}m$ phases are stable above 1400 and 2600 K and the two orthorhombic *Pbca* and *Pnma* phases above 3 and 20 GPa, respectively.[9–14] The given values are highly dependent on the actual state of aggregation (monocrystals versus polycrystalline aggregates) as well as on the thermal and loading history, purity, etc. As these five zirconia structures are centrosymmetric, they are all nonpolar and nonpiezoelectric. The transitions among the various ZrO_2 phases are also very interesting.

Owing to its widespread use and technological importance zirconia has been heavily studied both experimentally and theoretically. Unfortunately, its experimental investigation is particularly difficult. The cubic and tetragonal phases require high to very high amounts of dopants (up to 40% in molar content) to be stabilized at ambient conditions; this leaves open the question of the influence of such doping on the measured properties.[15,16] The monoclinic phase is prone to twinning; it is therefore difficult to grow large homogeneous crystals required for elasticity measurements.[9,17] Finally, the two orthorhombic phases are stable at high pressure (even though the *Pnma* phase can be recovered at ambient conditions[11,12]), making *in situ* neutron-diffraction studies somewhat impractical while x-ray diffraction is known not to be very sensitive for oxides.[9,18] All this contributes to explain why, to this day, many fundamental aspects of zirconia mechanics have not been completely elucidated; for instance, the phase diagram at high pressures and temperatures is still largely unknown, the exact microstructural mechanisms of many of its phase transitions are still unclear, and even the experimental values of the elastic moduli of the pure phases are not all very well characterized.

The theoretical knowledge of zirconia is consequently still incomplete as it is often "[…] not clear with which of the different experimental data the theory must agree […].[19]" Semi- or fully-empirical models have been used with success for several purposes;[8,19–22] first-principles methods have been used as well for studying the structural, electronic, or vibrational properties.[4,23–31] However, no detailed investigations have been performed on the elastic constants of ZrO_2 through a state-of-the-art first-principles approach. This is therefore the main purpose of the present paper. We aim at filling this gap in basic knowledge through a careful theoretical analysis in view also of providing useful benchmarks which may help future experimental work in this area. We take advantage of the recent theoretical framework[32] proposed for computing elastic properties, which here we also compare directly with more classical methods (see for instance Refs. 33–37 and the references therein).

After the brief description of an empirical model showing the limitations of an ionic approach for zirconia (Sec. II), we present the three pseudopotentials used in this paper to compute the structural and elastic properties of ZrO_2, as well as the computational setup (Sec. III). The five polymorphs represented in Fig. 1 are examined in turn; the resulting properties are then discussed and compared with available experimental and computational data (Sec. IV).

II. EMPIRICAL IONIC MODEL

Empirical potentials widely used for oxides belong to the Born-Mayer family,[8,40–43] with pair potentials $V_{ij}(r)$ for ions i and j of the form

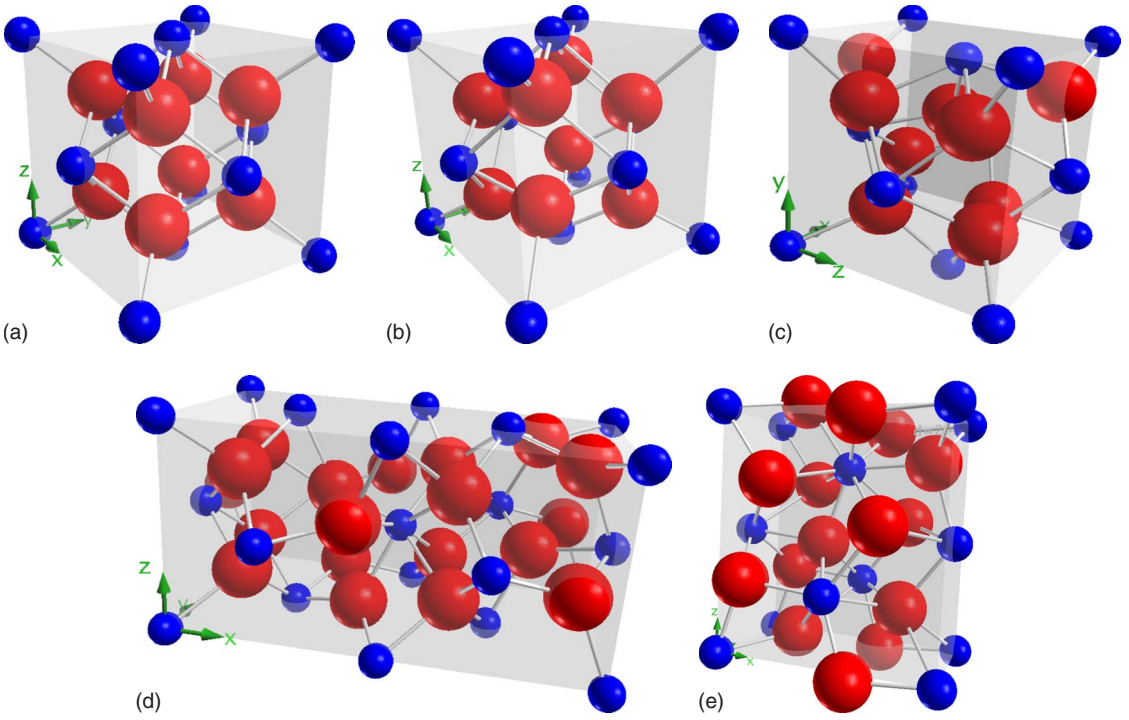

FIG. 1. (Color online) Primitive cells (except for $Fm\bar{3}m$ and $P4_2/nmc$, for which the face-centered cell is shown) of the five zirconia polymorphs investigated in the present paper. Pictures are to scale with ions depicted at half scale (data on ionic radii from Ref. 38): zirconium ions in dark gray (blue) and oxygen ions in light gray (red). For the tetragonal $P4_2/nmc$ structure, only the cubic axes are shown (see Appendix A). The coordination number is 8 for the $Fm\bar{3}m$ and $P4_2/nmc$, 7 for the $P2_1/c$ and *Pbca*, and 9 for the *Pnma* phases. All polymorphs retain the face-centered layout, with more or less deformation of the cubic phase. Pictures drawn with crystalOgraph.[39]

$$V_{ij}(r) = \frac{Z_i Z_j e^2}{r^2} + A_{ij} \exp\left(-\frac{r}{\bar{r}_{ij}}\right) - \frac{C_{ij}}{r^6}, \qquad (1)$$

where $Z_i e$ is the electric charge of ion i and the coefficients A_{ij}, C_{ij}, and $\bar{r}_{ij}$ pair-dependent parameters to be fitted to experiment.

This interaction is used in conjunction with a breathing ion model for oxygen: a distinction is made between the core (nucleus+core electrons) and the shell (valence electrons), which models the polarizability of oxygen. Static computations using the GULP package[44] similar to those described in Sec. III B below enable the determination of the structural and elastic parameters. The results for the potential defined in Eq. (1) as parametrized by Lewis and Catlow,[40] for $T=0$ K and $p=0$ Pa, are referred to as LC in all the following tables. Other parametrizations have also been studied,[8,41] resulting in no significant differences.

The lattice parameters are all correctly reproduced (see Sec. IV) with a precision comparable to first-principles computations. On the contrary, ionic coordinates are not always as accurate, showing evidence of missing physical features in the empirical model. This is especially true of the first group of oxygen ions in the monoclinic structure and even more so of the orthorhombic *Pbca*. Furthermore, the elastic constants are typically overestimated [a feature shared by the purely electrostatic potential induced breathing (PIB) model[45]], with few exceptions (such as the tetragonal C_{33}).

The main problem with the potential given in Eq. (1) is the predicted relative energetics of the phases; contrary to observations (see Sec. IV), the sequence from most to least stable is found to be: cubic, tetragonal, monoclinic, orthorhombic *Pbca*, and orthorhombic *Pnma*. This is in line with the predictions of the PIB model giving the sequence as cubic, orthorhombic *Pnma*, orthorhombic *Pbca*, tetragonal, and monoclinic.

This result confirms the work of Ho (Ref. 46) stating the mixed covalent-ionic character of the Zr-O bond in zirconia thereby requiring a quantum-mechanical description of the interactions.

III. COMPUTATIONAL DETAILS

The following computations have been performed with the open-source package ABINIT.[47–49] Three different sets of pseudopotentials have been used (see below), based on all-electron scalar-relativistic computations using the Perdew-Burke-Ernzerhof (PBE) exchange-correlation functional[50] and including nonlinear partial core corrections according to the scheme of Louie, Froyen, and Cohen[51] for zirconium [r_{core} varying from 0.8 (TM, RRKJ) to 1.2 a.u. (PAW)]. We remark that there is indeed a significant overlap of the core and valence charge densities between 0.4 and 1.2 a.u. away from the nucleus. Zirconium is also characterized by strong overlap of the 4*s*, 4*p*, and 4*d* wave functions; consequently, as discussed elsewhere,[3,26,52,53] the *N* shell must be included in the valence electrons in order to obtain reasonably accurate lattice parameters.

TABLE I. Comparison between the energy-interpolation (EI), finite-difference (fD), and the elastic-response (Ref.32) (ER) methods for the TM set of pseudopotentials in the cubic and tetragonal cases. The cutoff energy is indicated after the name of each phase; the BZ is sampled with a $4\times4\times4$ Monkhorst-Pack grid. Interpolation is done with 21 points and a maximal linear deformation equal to 10^{-2} for the elastic constants C_{ij} and 10^{-1} for the Birch-Murnaghan equation of state used to compute the bulk modulus B_0.

	Cubic (40 Ha)			Tetragonal (80 Ha)		
Parameter	EI	fD	ER	EI	fD	ER
C_{11} (GPa)	517.6 ± 0.4	526.8	533.5	422.5 ∓ 1.1	433.1	439.4
C_{33}				245.3 ± 8.8	257.8	264.3
C_{44}	61.69 ± 2.20	62.58	64.36	10.98 ± 0.12	10.04	37.45
C_{66}				62.07 ± 0.08	62.89	68.99
C_{12}	88.31 ∓ 0.05	94.17	97.86	112.9 ∓ 1.2	124.2	127.6
C_{13}				50.72 ∓ 0.65	56.63	59.99
B_0	231.4 ± 0.1	238.4	243.7	168.8 ± 0.2	177.7	182.0

A. Pseudopotentials, sampling, cutoff energy

"PAW" set. The first pseudopotential set was built using the Vanderbilt ultrasoft scheme[54] and recast in the projected augmented wave (PAW) formalism;[55–58] the USPP,[59] and USPP2ABINIT[60] packages were used to generate the potentials.

For both atomic species, the reference configuration is that of the neutral atom. For Zr the complete $n=4$ shell and the $5s$ subshell constitute the valence electrons; the cutoff radii for the s, p, and d subshells are 1.8, 2.0, and 2.2 a.u., respectively. For O the valence electrons are those of the $2s$ and $2p$ subshells with a cutoff radius of 1.1 a.u. for both.

These two pseudopotentials used together are hereafter referred to as PAW. It should be noted that the ultrasoft potentials on which the PAW set is based are those of Vanderbilt's USPP package [with the PBE in lieu of the Perdew-Wang 91 (Ref. 61) exchange-correlation functional] and that they also appear as such in the QUANTUM-ESPRESSO[62,63] distribution.

"RRKJ" set. The second set of pseudopotentials was built from scratch using the norm-conserving Rappe-Rabe-Kaxiras-Joannopoulos optimized scheme[64] and the OPIUM pseudopotential generator;[65] the reference configuration for zirconium was chosen to be that of the Zr^{4+} ion with the $4s$, $4p$, $4d$, and $5s$ states as valence and cutoff radii of 1.68, 1.73, 1.79, and 1.72 a.u., respectively, whereas the oxygen configuration is exactly as above with 1.53 and 1.6 a.u., respectively, for the cutoff radii of the s and p subshells. $l=3$ and $l=0$ are the local components for Zr and O, respectively.

"TM" set. The third set, built using the FHI98PP[66] package is based on the same reference configuration as for the PAW set; the Troullier-Martins norm-conserving scheme was used to generate the potentials. Cutoff radii are as for the RRKJ set. The local component is chosen to be $l=2$ for both atoms.

For any of the above sets, the pseudopotentials have been given relatively small cutoff radii in order to avoid large overlaps, considering that the Zr-O distance in all phases is typically between 3.6 and 4.2 a.u. (see in particular the discussion in Ref. 29, Sec. IIIC, about Ref. 26). The Brillouin zone (BZ) is sampled using the Monkhorst-Pack[67] scheme with a $4\times4\times4$ grid and the cutoff energy of the plane-wave expansion is fixed at $E_{\text{cut}}=60$ (PAW and RRKJ) or 80 Ha (TM), unless otherwise stated.

B. Computations of structural and elastic parameters

Structural parameters are found by minimizing the total energy with respect to symmetry-preserving deformations and ionic displacements; ABINIT includes a Broyden-Fletcher-Goldfarb-Shanno minimization scheme (BFGS). Initial values for the minimization were taken from available experiments.

Elastic parameters have been computed using either energy-interpolation or finite-difference methods,[33–35] the second being faster but less accurate, as forces and stresses are not variational quantities in the Kohn-Sham formalism. However, an increasing number of deformations is required as the symmetry of the structure is lowered and many points must be computed to obtain a reasonable interpolation: the computation time thus increases considerably. Details on both methods can be found in Refs. 33–37.

ABINIT also includes the treatment of response functions; elasticity is implemented according to the framework laid out in Ref. 32. It should be noted that the given expressions for the mixed second derivatives of the energy [Eqs (15) and (16)] are nonstationary (exactly as forces and stresses) and the formalism is valid for norm-conserving pseudopotentials only. The finite-difference method was therefore used preferentially for overall consistency; following the recommendations of Ref. 32, a tight limit of 10^{-10} Ha bohr^{-1} for interionic forces was imposed to obtain accurate elastic moduli.

Table I shows a comparison between the various methods

TABLE II. Relative energetics of zirconia polymorphs. The tabulated values give the difference of configurational energy (in meV/atom, repeated for each set of pseudopotentials) with respect to the monoclinic phase. $E_{\text{cut}}=30$ (PAW, RRKJ) or 40 Ha (TM).

Phase	PAW	RRKJ	TM
Monoclinic $P2_1/c$	0	0	0
Orthorhombic $Pbca$	+22.56	+16.51	+28.55
Tetragonal $P4_2/nmc$	+36.99	+53.22	+41.16
Cubic $Fm\bar{3}m$	+71.59	+80.98	+79.77
Orthorhombic $Pnma$	+114.5	+108.0	+135.6

TABLE III. Elastic properties of the zirconia polymorphs: linear compressibilities in 10^{-3} GPa^{-1}. The index of χ indicates the direction or set of equivalent directions. US: ultrasound velocity measurements. XRD: x-ray diffraction; EDXRD: energy-dispersive XRD; ADXRD: angular-dispersive XRD. ND: neutron diffraction. BS: Brillouin scattering; BS/US: combined BS/ultrasound measurements. The cutoff energy is 60 (PAW, RRKJ) or 80 Ha (TM), unless otherwise stated. The tetragonal compressibilities are the same in the primitive tetragonal and in the conventional cubic axes, see Appendix A.

Cubic $Fm\bar{3}m$

Source	$\chi_{\langle 100\rangle}$
US (Ref .15)	1.72
HF (Ref. 24)	1.50
TB Ref. 21	1.08
PIB (Ref.45)	1.16
LD (Ref. 20)	1.72
LD (Ref. 19)	1.94
PAW (90)	1.42
RRKJ (120)	1.40
TM	1.37

Tetragonal $P4_2/nmc$

Source	$\chi_{\langle 100\rangle}$	$\chi_{[001]}$
XRD (Ref. 72)	1.41	2.24
ND (Ref.16)	1.91	2.88
TB (Ref. 21)	1.44	2.69
PIB (Ref. 45)	1.59	2.59
LD (Ref. 20)	1.92	1.83
LD (Ref. 19)	1.75	3.26
LD (Ref. 73)	3.04	2.15
PAW (90)	1.51	3.40
RRKJ (120)	1.47	3.32
TM (120)	1.47	3.24

Monoclinic $P2_1/c$

Source	$\chi_{[100]}$	$\chi_{[010]}$	$\chi_{[001]}$	χ_{β}
XRD (Refs. 74 and 75)	6.2	2.0	7.5	
ND (Ref. 76)	3.4	1.0	5.0	
EDXRD (Ref.77)	3.3	3.1	2.6	
XRD (Refs. 9 and 78)	2.92	2.97	2.20	0.272
BS (Ref. 17)	2.69	–0.27	3.68	–0.765
BS/US (Ref. 79)	1.86	0.48	3.48	–0.698
LD (Ref. 19)	1.91	0.824	2.54	0.402
PAW	2.12	0.866	2.62	0.476
RRKJ	2.04	0.725	2.61	0.424
TM	2.10	0.781	2.64	0.454

Orthorhombic $Pbca$

Source	$\chi_{[100]}$	$\chi_{[010]}$	$\chi_{[001]}$
ADXRD (Ref. 80)	0.72 ± 0.16	1.51 ± 0.43	2.84 ± 0.74
PAW (30)	1.64	1.35	1.80
RRKJ (30)	1.61	1.33	1.57
TM (40)	1.63	1.36	1.78

Orthorhombic $Pnma$

Source	$\chi_{[100]}$	$\chi_{[010]}$	$\chi_{[001]}$
ADXRD (Ref. 11)	0.89(2)	0.76(3)	1.04(3)
LD (Ref. 19)	1.05	1.58	1.31
PAW	0.81	2.31	1.7
RRKJ	1.22	1.64	1.32
TM	0.81	2.30	1.74

for the TM set in the cubic and tetragonal cases. Results are similar with differences not exceeding 10% across the table except for the tetragonal moduli C_{13} and C_{44}.

C. Convergence properties

Two types of convergence are checked: convergence of the lattice parameters and of the elastic moduli. For reasons of computational cost a full investigation of the convergence with respect to the number of grid points has been undertaken for the cubic case only; there is virtually no dependence on the grid density. Some computations done in the tetragonal case showed however a dependence comparable to the influence of the cutoff energy. Results for $E_{\mathrm{cut}}=30$ Ha and a $10\times10\times10$ Monkhorst-Pack grid remain within 2.5% of those obtained for $E_{\mathrm{cut}}=90$ Ha and a $4\times4\times4$ grid.

Structural parameters, as it is well known, converge quickly even with moderate values of the cutoff energy; in the most unfavorable case (RRKJ set), the relative differences between the computations done with the lowest and highest cutoff energies do not exceed 0.5%.

Accurate values of the elastic constants require a higher cutoff. The RRKJ set shows a uniformly slow convergence while the other two are better behaved; in the tetragonal case however, convergence is more difficult to reach even for the PAW set of potentials.

IV. RESULTS AND DISCUSSION

A. Relative energetics of polymorphs

The monoclinic phase is found to have the minimum ground-state energy (see Table III), in agreement with experimental data. In order of increasing ground-state energy are then found: the orthorhombic *Pbca*, tetragonal, cubic, and orthorhombic *Pnma* polymorphs. This agrees with the ordering given by Refs. 21 and 30 and the partial ordering of Refs. 26, 29, and 68 but is in contrast with the findings of Ref. 69, which places the two orthorhombic phases at a lower energy than the monoclinic polymorph.

We notice that the hierarchy of relative stability (monoclinic, orthorhombic *Pbca*, then tetragonal) found by the computations at $T=0$ K and $p=0$ Pa, as reported in Table II, agrees better with the experimentally observed behavior of zirconia when raising pressure at constant room temperature

TABLE IV. Structural and elastic properties of cubic zirconia computed by finite differences. The ionic positions are given in reduced contravariant coordinates. Wyckoff positions[82] are indicated after the name of the atoms. Exp.: experimental data; LC, PAW, RRKJ, TM: present work, see text; TB: tight binding; LD: lattice dynamics; HF: Hartree-Fock; PIB: potential-induced breathing. In the LC case, ionic coordinates were fixed at the experimental values. E_{cut}=60 (PAW, RRKJ) or 80 Ha (TM) unless otherwise stated.

					Cubic $Fm\bar{3}m$						
Parameter	Expt. (Ref. 81)	LC	PAW	RRKJ	TM	LDA (Ref. 4)	LDA (Ref. 29)	PW91 (Ref. 26)	TB (Ref. 21)	LD (Ref. 19)	GGA (Ref. 30)
a (nm)	0.50858	0.5096	0.5116	0.5111	0.5107	0.5037	0.5037	0.5164	0.5020	0.523	0.51280

					Cubic $Fm\bar{3}m$					
Parameter	Expt. (Ref. 15)[a]	LC	PAW (90)	RRKJ (120)	TM	HF (Ref. 24)	TB (Ref. 21)	PIB (Ref. 45)	LD (Ref. 20)	LD (Ref.19)
C_{11} (GPa)	417	630	520	522	526	628	543	548	455	409
C_{12}	82	152	93.1	96.5	95.2	19	193	158	64	53
C_{44}	47	100	61.4	63.9	62.8	82	57	180	63	60
B_0	194	311	235	238	239	222	310	288	194	171

[a]Extrapolation at zero yttria content.

rather than when raising temperature at constant room pressure (see the phase diagrams of Refs. 2, 9, 70, and 71).

B. Cubic $Fm\bar{3}m$ phase

The cubic polymorph, isostructural to fluorite CaF_2 (number Z of formula units per primitive cell equal to 1) is characterized by Zr ions at Wyckoff position 4a (0,0,0) and O ions at position 8c (1/4,1/4,1/4); each Zr^{4+} ion is coordinated with 8 O^{2-} ions.

The computations show that the cubic phase is unfavored (the ground-state energy ranging from +70 to +80 meV/atom with respect to that of the monoclinic phase); only the orthorhombic *Pnma* has a higher ground state. Structural data are correctly reproduced as summarized in Table IV.

There has been much discussion about the influence of dopants (especially yttria) on the elastic properties of this phase; the present work agrees with the observations of Ref. 29 on the reduction (for doped cubic zirconia) of the elastic moduli, yielding a large difference (+25%) for C_{11}, and consequently for the bulk modulus B_0, and with Ref. 30 which reports, also from first-principles computations, B_0=251 GPa.

Another interesting information is the anisotropy coefficient $(C_{11}-C_{12})/(2C_{44})$ as evaluated by Brillouin scattering and ultrasound measurements;[83,84] by extrapolating the mass content of yttria to zero, the above coefficient is found to be 3.62 ± 2.05 (the lack of data points being responsible for the large error). The present computed values for PAW, RRKJ, and TM are 3.55, 3.35, and 3.38, respectively, in good agreement with experimental data.

It is also useful to consider the linear compressibilities χ_i, $i=1,2,3$, defined as

$$\chi_i = \sum_{j=1}^{3} S_{ij},$$

where S is the compliance matrix and i refers to the Cartesian axes as usual, i.e., $i=1 \rightarrow [100]$, $i=2 \rightarrow [010]$, and $i=3 \rightarrow [001]$. Linear compressibilities are easily computed from experiment when the pressure is varied, enabling a direct comparison between computations and experimental data. Results are given in Table III; the present computations are consistent with the experimental data which, however, are quite scattered.

C. Tetragonal $P4_2/nmc$ phase

The tetragonal polymorph is composed of Z=2 f.u. per primitive cell; Zr and O ions are in Wyckoff position 2a(3/4,1/4,3/4) and 4d$(1/4,1/4,z)$, respectively, z=0 corresponding to the cubic phase. The tetragonal phase can also be represented by a face-centered cell with twice the volume of the primitive cell (see Fig. 1 and Appendix A), which shows most clearly that the columns of O ions are displaced alternately "up" and "down" with respect to their positions in the cubic fluorite structure; these displacements are the eigenvectors of the X_2^- cubic mode.[85]

The tetragonal polymorph is stable only between approximately 1400 and 2650 K; the lower bound is highly dependent on the thermal and load history of the sample.[70,71,86–93] Dopants (principally magnesia MgO and ceria CeO_2) are used in lesser proportions than for the cubic polymorph (typically 10% mol or less).

The calculated structural parameters are in good agreement with experiment for a and the free internal parameter z; c is slightly overestimated, exactly as in Ref. 26 but is still within 2% of the experimental value.

The elastic moduli have been computed in the conventional cubic axes [value indicated with a (c) in Table V], in order to compare computations for the various polymorphs. The corresponding transformation from the primitive tetragonal axes is described in Appendix A. Apart from Refs. 19 and 20, the cited works do not explicitly state which Cartesian axes are used; we have therefore indicated the elastic constants in the primitive tetragonal axes too [value indicated with a (t) in Table V]. The computed elastic properties

TABLE V. Structural and elastic properties of tetragonal zirconia; see key of Table IV. [ER] indicates that the ABINIT elastic response module was used to compute the elastic properties. (c) indicates that the elastic constant is given in the cubic axes, (t) in the primitive tetragonal axes, and no indication means that the chosen set of axes is unknown; see Appendix A for details.

			Tetragonal $P4_2/nmc$ (origin choice 2)									
Parameter	Exp. (Ref. 81)	LC	PAW	RRKJ	TM	LDA (Ref. 4)	LDA (Ref. 29)	PW91 (Ref. 26)	TB (Ref. 21)	LD (Ref. 19)	GGA (Ref. 30)	
a (nm)	0.36055	0.3618	0.3622	0.3616	0.3614	0.3557	0.3565	0.3654	0.3571	0.36370	0.36287	
c (nm)	0.51797	0.5196	0.5284	0.5271	0.5272	0.5100	0.5126	0.5364	0.5184	0.52689	0.52070	
O (4d) z	0.057	0.010	0.05725	0.05560	0.05680	0.0418	0.0441	0.060	0.047		0.040	
					Tetragonal $P4_2/nmc$							
Parameter	Exp. (Ref.17)[a]	Exp. (Ref. 16)	LC	PAW (90)	RRKJ (120[ER])	TM	TB (Ref. 21)	PIB (Ref. 45)	LD (Ref. 20)	LD (Ref. 19)	LD (Ref. 73)	
C_{11} (GPa)	340	327	546(c)/441(t)	424(c)/334(t)	432 (c)/346(t)	433(c)/342(t)	366	465	395(c)	416(c)	263	
C_{33}	325	264	287(c/t)	248(c/t)	252(c/t)	258(c/t)	286	326	326(c)	234(c)	262	
C_{44}	66	59	49.3(c/t)	9.08(c/t)	32.2(c/t)	10.0(c/t)	78	101	42(c)	39(c)	55.9	
C_{66}	95	64	104(c)/209(t)	61.3(c)/152(t)	68.2 (c)/154(t)	62.9(c)/154(t)	88	156	56(c)	73(c)	44	
C_{12}	33	100	127(c)/233(t)	121(c)/211(t)	124 (c)/210(t)	124(c)/216(t)	180	83	26(c)	30(c)	15	
C_{13}	160	62	53.9(c/t)	51.9(c/t)	55.5(c/t)	56.6(c/t)	80	49	105(c)	68(c)	72	
B_0	183	149	205	172	176	182	190	179	148	134	122	

[a]Extrapolation at 1480 K.

are far more at variance with experiment than for the cubic case; experimental difficulties (for instance microtwinning[16]) and the necessity to use doped crystals[16] may all be sources of divergence with the first-principles computations.

Table III shows a good convergence on compressibility along the ⟨100⟩ direction whereas there is serious disagreement for the orthogonal direction [001] (from 1.8×10^{-3} GPa^{-1} to nearly twice as much); however, except for Ref. 73, the [001] direction is given as being more compressible than the ⟨100⟩ direction. The tetragonal phase shows a high degree of elastic anisotropy in contrast to the cubic phase of which it is a slight deformation; see the discussion at the end of the next paragraph. As pointed out by Refs. 19 and 20, it is natural to relate this anisotropy to the deformed coordination octahedron of the zirconium ion; a detailed electronic analysis (for instance with the electron localization function as done in Ref. 94 for ReB_2) may help obtain a better understanding of this issue.

D. Monoclinic $P2_1/c$ phase

The monoclinic polymorph, while retaining the face-centered layout of the cubic and tetragonal phases, shows considerable distortion; the coordination number for Zr decreases to 7. There are $Z=4$ f.u. per primitive cell; Zr cations (one set of ions) and O anions (two sets) are all in Wyckoff position 4e(x,y,z).

As mentioned in Sec. I, baddeleyite is prone to twinning on both {100} and {110} sets of equivalent planes, and is therefore difficult to grow in macroscopic monocrystals necessary for experimental studies.

All structural parameters are well reproduced, including the internal atomic positions; the only relevant difference is for the monoclinic angle β, which is slightly overestimated with respect to experiment and some other computations, but in close agreement with Refs. 29 and 30.

The elastic coefficients are computed in the basis indicated in Fig. 2. They are in fair agreement with experimental data for the diagonal part. Off-diagonal terms are less accurate, in particular C_{13} and the C_{i5}, $i=1,2,3$ (wrong sign or magnitude or both; see however the comment on χ_2 below); this is still in line with published results, see Table VI.

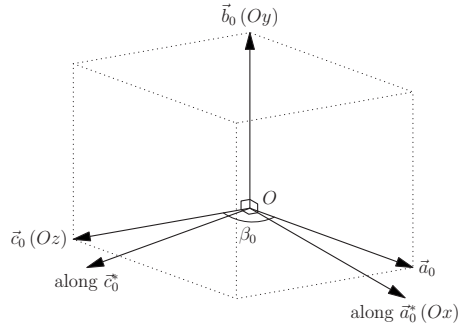

FIG. 2. Undeformed monoclinic cell (in dashed lines). The Cartesian reference frame (O,x,y,z) where the elastic moduli are computed is along $\vec{a}_0^*$ (reciprocal vector of $\vec{a}_0$), $\vec{b}_0$, and $\vec{c}_0$; these are the Cartesian axes used in Ref. 17.

TABLE VI. Structural and elastic properties of monoclinic zirconia; see key of Table IV.

		Monoclinic $P2_1/c$										
Parameter		Exp. (Ref. 75)	Exp. (Ref. 95)	Exp. (Ref. 81)	LC	PAW	RRKJ	TM	LDA (Ref. 4)	LDA (Ref. 29)	PW91 (Ref.26)	TB (Ref. 21)	GGA (Ref. 30)
a (nm)		0.5169	0.51450	0.51505	0.5122	0.5190	0.5191	0.5180	0.5108	0.5102	0.5192	0.5076	0.51974
b (nm)		0.5232	0.52075	0.52116	0.5202	0.5243	0.5238	0.5231	0.5170	0.5181	0.5254	0.5081	0.52798
c (nm)		0.5341	0.53107	0.53173	0.5315	0.5379	0.5365	0.5370	0.5272	0.5264	0.5358	0.5172	0.53498
β (°)		99.25	99.23	99.230	98.34	99.65	99.68	99.61	99.21	99.65	99.23[96]	98.00	99.53
Zr (4e)	x	0.2758	0.2758	0.2754	0.2585	0.2758	0.2764	0.2756	0.2769	0.2776	0.2773	0.272	0.276
	y	0.0404	0.0411	0.0395	0.02142	0.04372	0.04218	0.04342	0.0422	0.0427	0.0416	0.027	0.043
	z	0.2089	0.2082	0.2083	0.2288	0.2100	0.2087	0.2103	0.2097	0.2092	0.2103	0.217	0.207
O (4e)	x	0.069	0.0703	0.0700	0.03983	0.06513	0.06652	0.06480	0.0689	0.0704	0.071	0.078	0.071
	y	0.342	0.3359	0.3317	0.2743	0.3266	0.3287	0.3257	0.3333	0.3372	0.336	0.336	0.336
	z	0.345	0.3406	0.3447	0.4162	0.3498	0.3477	0.3507	0.3445	0.3407	0.341	0.342	0.342
O (4e)	x	0.451	0.4423	0.4496	0.4728	0.4509	0.4508	0.4511	0.4495	0.4482	0.448	0.452	0.448
	y	0.758	0.7549	0.7569	0.7521	0.7568	0.7570	0.7566	0.7573	0.7576	0.757	0.752	0.758
	z	0.479	0.4789	0.4792	0.4678	0.4755	0.4774	0.4754	0.4798	0.4807	0.479	0.472	0.480

	Monoclinic $P2_1/c$							
Parameter	Exp. (Ref. 17)	Exp. (Ref. 79)	LC	PAW	RRKJ	TM	PIB (Ref. 45)	LD (Ref. 19)
C_{11} (GPa)	361	358	389	337	353	337	353	347
C_{22}	408	426	426	351	380	354	434	364
C_{33}	258	240	355	268	275	267	272	274
C_{44}	99.9	99.1	113	79.1	92.1	77.2	156	88
C_{55}	81.2	78.7	106	70.3	74.4	70.3	123	108
C_{66}	126	130	132	114	119	113	192	122
C_{12}	142	144	233	155	157	157	233	164
C_{13}	55.0	67.0	154	84.3	87.5	88.8	138	102
C_{15}	−21.3	−25.9	39.3	25.9	28.1	25.7	61	28
C_{23}	196	127	145	153	161	156	191	156
C_{25}	31.2	38.3	23.4	−4.28	−8.62	−4.32	−44	−17
C_{35}	−18.2	−23.3	13.6	1.91	0.0520	0.695	59	11
C_{46}	−22.7	−38.8	−18.6	−14.6	−16.7	−15.2	−35	−44
B_0	201	189	248	193	202	196	182	194

TABLE VII. Structural and elastic properties of orthorhombic Pbca zirconia; see key of Table IV.

		Orthorhombic *Pbca*						
Parameter	Exp.(Ref. 10)	LC	PAW (30)	RRKJ (30)	TM (40)	LDA (Ref. 3)	TB (Ref 21)	GGA (Ref. 30)
a (nm)	1.00861	1.0107	1.0150	1.0083	1.0131	1.0086(Ref. 10)	0.99152	1.01745
b (nm)	0.52615	0.5248	0.5299	0.5333	0.5290	0.52650(Ref.10)	0.51559	0.53148
c (nm)	0.50910	0.5119	0.5132	0.5137	0.5123	0.50934(Ref.10)	0.50667	0.51357
Zr (8c) x	0.8843	0.875	0.8843	0.8852	0.8843	0.8848	0.880	0.885
y	0.0332	0	0.03489	0.03679	0.03470	0.0357	0.002	0.035
z	0.2558	0.25	0.2519	0.2597	0.2522	0.2531	0.256	0.253
O (8c) x	0.9779	1	0.9781	0.9778	0.9782	0.9779	0.978	0.977
y	0.7477	0.75	0.7388	0.7373	0.7387	0.7393	0.745	0.739
z	0.4948	0.5	0.4977	0.4974	0.4975	0.4989	0.509	0.497
O (8c) x	0.7911	0.75	0.7888	0.7888	0.7887	0.7895	0.784	0.790
y	0.3713	0.25	0.3728	0.3728	0.3727	0.3740	0.371	0.375
z	0.1310	0	0.1247	0.1307	0.1245	0.1268	0.131	0.127

	Orthorhombic *Pbca*			
Parameter	LC	PAW (30)	RRKJ (30)	TM (40)
C_{11} (GPa)	417	349	377	349
C_{22}	484	397	420	393
C_{33}	424	352	404	355
C_{44}	130	87.1	97.5	86.2
C_{55}	125	84.3	110	83.5
C_{66}	156	115	133	116
C_{12}	222	150	151	152
C_{13}	188	125	123	124
C_{23}	164	120	127	121
B_0	275	210	222	210

Data on linear compressibilities can be found in Table III; the expression of $\chi_\beta = -(1/\beta_0)\partial\beta/\partial p$ is given in Appendix B, whereas the computations of the compressibilities along $[100]_m$ and $[001]_m$ require a change of Cartesian axes (see Fig. 2). The monoclinic phase shows a high elastic anisotropy for nearly all the cited references, except for Ref. 9: the compressibilities in the $[100]_m$ and $[001]_m$ directions are given as having approximately the same magnitude, while being two or three times larger than the compressibility along the twofold axis $[010]_m$.

The monoclinic angle β is found to increase as pressure is applied, according to Refs. 17 and 79. Conversely, present calculations and other experiments[9] predict the opposite trend. Of note is the unphysical negative value of χ_2 found experimentally in Ref. 17, which illustrates the difficulties faced when measuring elastic constants.

A comparison of the computed elastic properties of the cubic, tetragonal, and monoclinic phases shows that there is a gradual decrease, from cubic to monoclinic, in the value of C_{11} (from ≈520 to ≈350 GPa), while a distinct elastic anisotropy appears with the tetragonal and monoclinic polymorphs, the terms of each of the pairs C_{11} and C_{33}, C_{44} and C_{66}, and C_{12} and C_{13} being quite different in magnitude. In contrast with the other two polymorphs, the tetragonal phase has a low shear modulus, as seen from the values of the moduli C_{44} and C_{66}.

E. Orthorhombic *Pbca* phase

The first of the two orthorhombic phases, often referred to as *Ortho-I* in the literature (as it is the first polymorph found when increasing pressure), is isostructural to brookite TiO_2; this is the only known case for which zirconium and titanium have isostructural oxides. $Z=8$ f.u. is found per primitive cell; Zr ions (one set) and O ions (two sets) occupy all Wyckoff position 8c(x,y,z). The coordination number is 7; as can be seen from Fig. 1, this structure results from two deformed fluoritelike cells joined along the $[100]_o$ axis.

The calculated structural parameters compare fairly well with experiment and with the published computations (see Table VII). No experimental data appear available on elastic moduli except for the bulk modulus, evaluated at 220 GPa from a Birch-Murnaghan fit;[9] agreement is excellent with the present work, as well as with Ref. 30, which reports a value of 204 GPa also from first-principles computations. There exist however data on linear compressibilities, as shown in Table III.

The discrepancies found in the table might be explained by: (i) The low energy cutoff (30 or 40 Ha); however, at least

TABLE VIII. Structural and elastic properties of orthorhombic *Pnma* zirconia; see key of Table IV.

		Orthorhombic *Pnma*									
Parameter		Exp. (Ref 11)	Exp. (Ref. 12)	LC	PAW	RRKJ	TM	LDA (Ref. 28)	PW91 (Ref. 26)	TB (Ref. 21)	GGA (Ref. 30)
a (nm)		0.5741	0.55873	0.5519	0.5599	0.5603	0.5591	0.5598	0.5668	0.55781	0.56140
b (nm)		0.3246	0.33298	0.3512	0.3375	0.3363	0.3370	0.3340	0.3361	0.33022	0.33474
c (nm)		0.6341	0.64847	0.6639	0.6549	0.6530	0.6537	0.6553	0.6591	0.63534	0.65658
Zr (4c)	*x*	0.251	0.2459	0.2565	0.2490	0.2474	0.2489	0.247	0.2532	0.255	0.246
	z	0.109	0.1108	0.08360	0.1071	0.1104	0.1072	0.118	0.1115	0.099	0.113
O (4c)	*x*	0.364	0.3599	0.3723	0.3610	0.3606	0.3611	0.360	0.3602	0.354	0.360
	z	0.422	0.4248	0.4027	0.4223	0.4248	0.4231	0.429	0.4253	0.421	0.425
O (4c)	*x*	−0.021	−0.0250	0.01969	−0.0212	−0.02340	−0.02139	−0.028	−0.0233	−0.022	−0.024
	z	0.672	0.6612	0.6472	0.6586	0.6596	0.6586	0.667	0.6602	0.662	0.662

	Orthorhombic *Pnma*				
Parameter	LC	PAW	RRKJ	TM	LD (Ref. 19)
C_{11} (GPa)	578	422	421	426	463
C_{22}	340	293	369	293	400
C_{33}	223	327	388	335	429
C_{44}	85.2	52.4	74.3	56.6	31
C_{55}	44.5	69.9	84.5	70.7	113
C_{66}	114	117	109	118	126
C_{12}	146	145	147	147	165
C_{13}	154	178	184	181	193
C_{23}	51.4	114	160	118	149
B_0	205	213	240	216	254

for the PAW set, convergence is not really a problem; (ii) an insufficient sampling of the BZ (a problem not easily overcome, as computations on the orthorhombic *Pbca* structure with its 192 electrons are very time consuming); (iii) the fact that x-ray diffraction measurements were used in the experiment of Ref. 9. While this is not as precise as neutron diffraction, errors are not expected to be large. However, the x-ray diffraction pattern could be indexed on a wrong structure because the low scattering factor of oxygen might lead to a confusion of otherwise distinguishable positions. Other experimental problems are listed in Ref. 9 and any of these might contribute to explain the divergence observed in Table III.

F. Orthorhombic *Pnma* phase

The second of the two orthorhombic polymorphs, often referred to as *Ortho-II* in the literature, is isostructural to cotunnite $PbCl_2$. $Z=4$ formula units are found per primitive cell; Zr ions (one set) and O ions (two sets) occupy all Wyckoff position $4c(x,1/4,z)$. The coordination number rises to 9; the zirconium sublattice is the most heavily deformed with respect to the fluorite prototype.

According to Ref. 11, the bulk modulus of the orthorhombic *Pnma* phase is 332 GPa, which would put this polymorph, along with the other oxides of the groups 4 and 8 (TiO_2, RuO_2, OsO_2), in the category of superhard materials; see Ref. 97 and references therein.

The *Pnma* phase is stable at high pressure: between 22 and 27 GPa for Ref. 9 (which however failed to identify the correct structure); at 18 and 26.7 GPa when heated, between 25 and 48.5 GPa unheated, and recovered at ambient conditions for Ref. 11. Reference 13 observed a transition from the orthorhombic *Pbca* structure at 13 GPa but they could not identify unambiguously the new structure. Finally, Refs. 72 and 98 report a transition between the orthorhombic *Pbca* and *Pnma* polymorphs at 22 GPa and above 25 GPa for nanocrystalline and polycrystalline zirconia, respectively.

The computed lattice parameters are in better agreement with Ref. 12 (measurements made with neutron diffraction) than with Ref. 11 (x-ray diffraction), see Table VIII; the latter is not as sensitive as the former for oxides because of the low scattering factor of oxygen.[9,18] All other published results are also closer to the neutron-diffraction experiment.

The computed elastic coefficients compare reasonably well with Ref. 19, with some exceptions, for instance, C_{22}; the PAW and TM sets give very similar results, with lower values for the diagonal coefficients than for Ref. 19 and the RRKJ set. These differences appear in the bulk modulus too, which in any case remains far lower than the experimental value of 332 GPa reported above,[11] while in agreement with another first-principles computation[30] reporting 251 GPa. As

it is well known, the generalized gradient approximation tends to predict larger values of the lattice parameters but lower values of the elastic constants than experimentally observed, whereas the local-density approximation does exactly the reverse (see for instance the results in Ref. 99); in the present case however, values of the bulk modulus do not exceed 278 GPa (Refs. 30 and 100) for the local-density approximation.

There is also a divergence regarding linear compressibilities, as seen in Table III. New experiments are necessary for a better understanding of this potentially interesting polymorph.

V. CONCLUSIONS

We have examined the structural and elastic properties of the five zirconia polymorphs, computing their complete stiffness matrices by first-principles methods. When feasible, the results of the different procedures for computing the elastic moduli were compared, resulting in overall good agreement (10% or less, with two exceptions); the finite-difference method proved to be a good compromise between accuracy and speed.

The three sets of pseudopotentials used in this paper converged toward similar values of the structural and elastic parameters, in close agreement with Refs. 26 and 30, where the generalized gradient approximation was also used. The elastic properties compare reasonably well with published results, except for the tetragonal phase.

The cubic phase is found to be harder than experimentally observed; conversely, the *Pnma* phase is softer. This is in accordance with other computations[19–21,24,29,30,45] but in disagreement with experiment.[11,12,98]

ACKNOWLEDGMENTS

We acknowledge the financial support by MiUR under project PON-"CyberSAR," and the project MATHMAT of the University of Padova. We thank F. Bernardini for numerous discussions, M. Dessalvi for his technical assistance, and A. S. Pereira for providing experimental data.

APPENDIX A: THE TETRAGONAL ELASTIC MODULI IN THE CONVENTIONAL CUBIC BASIS

It is sometimes convenient to compute the elastic moduli of the tetragonal phase in a system of Cartesian axes oriented along the conventional cubic axes ($[110]_t=[100]_c, [1\bar{1}0]_t=[010]_c, [001]_t=[001]_c$), where the t and c indices refer to the tetragonal and cubic phases, respectively. This enables a quick comparison between all polymorphs, which, as noted in Fig. 1, share the same face-centered layout of the cubic phase.

Let two sets e and e' of orthonormal basis vectors be related by an orthogonal transformation U,

$$e' = Ue \Leftrightarrow |e_i'\rangle = \sum_j |e_j\rangle\langle e_j|e_i'\rangle = \sum_j u_{ij}|e_j\rangle,$$

where $u_{ij}=\langle e_j|U|e_i\rangle=\langle e_j|e_i'\rangle$ are the components of U in the e basis. The components of a fourth-rank Cartesian tensor transform under the action of U according to

$$c'_{ijkl} = \sum_{mnpq} u_{im}u_{jn}u_{kp}u_{lq}c_{mnpq}. \tag{A1}$$

As a rotation of angle $\pi/4$ around $[001]_t$ is required to go from the primitive tetragonal to the conventional cubic axes, we get

$$U = \begin{pmatrix} 1/\sqrt{2} & 1/\sqrt{2} & 0 \\ -1/\sqrt{2} & 1/\sqrt{2} & 0 \\ 0 & 0 & 1 \end{pmatrix};$$

consequently, the components c^t_{ijkl} and c^c_{ijkl} of the tetragonal stiffness tensor are

$$c^c_{1111} = \frac{1}{2}(c^t_{1111} + c^t_{1122} + 2c^t_{1212}),$$

$$c^c_{1122} = \frac{1}{2}(c^t_{1111} + c^t_{1122} - 2c^t_{1212}),$$

$$c^c_{1212} = \frac{1}{2}(c^t_{1111} - c^t_{1122}),$$

the other components being the same in the two bases. It can be checked that another application of the same rotation gives back the original coefficients c^t_{ijkl}, as it should be by tetragonal symmetry (invariance by rotation of $\pi/2$ around $[001]_t$).

The compressibilities turn out to be the same in both sets of axes; indeed, we have

$$\chi^t_{\langle 100\rangle} = \frac{c^t_{3333} - c^t_{1133}}{(c^t_{1111} + c^t_{1122})c^t_{3333} - 2(c^t_{1133})^2},$$

$$\chi^t_{[001]} = \frac{c^t_{1111} + c^t_{1122} - c^t_{1133}}{(c^t_{1111} + c^t_{1122})c^t_{3333} - 2(c^t_{1133})^2},$$

and $c^c_{1111}+c^c_{1122}=c^t_{1111}+c^t_{1122}$.

APPENDIX B: DERIVATION OF χ_β

Let us consider the monoclinic cell, with zero-stress parameters a_0, b_0, c_0, and β_0, the Cartesian axes being z along $[001]_m$, y along $[010]_m$, and x orthogonal to both (i.e., along $\vec{a}_0^*$, see Fig. 2).

If we apply an isotropic load $\sigma=-p1$, where 1 is the identity matrix, the deformation is given by $e=S\sigma$, S being the compliance tensor; therefore

$$e_{ij} = -p\sum_{k=1}^{3} S_{ijkk}, \tag{B1}$$

with $e_{12}=e_{23}=0$ by monoclinic symmetry. In the preceding Cartesian basis, the deformation of the monoclinic cell under the application of pressure p is consequently

$$\begin{pmatrix} 1+e_{11} & 0 & e_{13} \\ 0 & 1+e_{22} & 0 \\ e_{13} & 0 & 1+e_{33} \end{pmatrix}\begin{pmatrix} a_0 \sin\beta_0 & 0 & 0 \\ 0 & b_0 & 0 \\ a_0\cos\beta_0 & 0 & c_0 \end{pmatrix} = \begin{pmatrix} [(1+e_{11})\sin\beta_0 + e_{13}\cos\beta_0]a_0 & 0 & e_{13}c_0 \\ 0 & (1+e_{22})b_0 & 0 \\ [e_{13}\sin\beta_0 + (1+e_{33})\cos\beta_0]a_0 & 0 & (1+e_{33})c_0 \end{pmatrix}.$$

To first order in deformation (i.e., up to linear terms in pressure), we have

$$\vec{a}\cdot\vec{c} = a_0c_0[(1+2e_{33})\cos\beta_0 + 2e_{13}\sin\beta_0],$$

where $\vec{a}$ and $\vec{c}$ (of respective magnitudes a and c) are the lattice vectors of the deformed monoclinic cell, and

$$a = a_0(1+e_{11}\sin^2\beta_0 + 2e_{13}\sin\beta_0\cos\beta_0 + e_{33}\cos^2\beta_0),$$

$$c = c_0(1+e_{33}).$$

The monoclinic angle β after deformation is therefore

$$\cos\beta = \frac{\vec{a}\cdot\vec{c}}{ac} = \cos\beta_0 + 2e_{13}\sin^3\beta_0 + (e_{33}-e_{11})\sin^2\beta_0\cos\beta_0,$$

and consequently

$$\sin\beta = \sin\beta_0(1-2e_{13}\sin\beta_0\cos\beta_0 - (e_{33}-e_{11})\cos^2\beta_0).$$

The pressure derivative of β is related to the angular compressibility χ_β by

$$\chi_\beta = -\frac{1}{\beta_0}\frac{\partial\beta}{\partial p} = \frac{1}{\beta_0\sin\beta}\frac{\partial\cos\beta}{\partial p},$$

which gives

$$\chi_\beta = -\frac{\sin\beta_0}{\beta_0}[(\kappa_{33}-\kappa_{11})\cos\beta_0 + 2\kappa_{13}\sin\beta_0] \tag{B2}$$

to first order in deformation, where

$$\kappa_{ij} = -\frac{\partial e_{ij}}{\partial p} = \sum_{k=1}^{3} S_{ijkk},$$

(supposing $\frac{\partial S}{\partial p} \ll \frac{S}{p}$) by Eq. (B1); κ_{33} is the linear compressibility χ_3 along $[001]_m$, κ_{11} along $\vec{a}_0^*$.

It can be checked that the value of χ_β is independent of the chosen Cartesian axes, provided the expression (B2) is modified accordingly: for instance, choosing x along $[100]_m$, y still along $[010]_m$, and z orthogonal to both (i.e., along $\vec{c}_0^*$), Eq. (B2) is modified by exchanging the indices 1 and 3; of course the compliance tensor must be recomputed in the new basis by using the transformation (A1).

*fadda@dsf.unica.it
†luciano.colombo@dsf.unica.it
‡zanzotto@dmsa.unipd.it

[1] A. Medevielle, F. Thévenot, and D. Tréheux, J. Eur. Ceram. Soc. **15**, 1193 (1995).
[2] *Zirconia Engineering Ceramics*, edited by E. H. Kisi (Trans Tech, Ütikon-Zürich, 1998).
[3] G. Stapper, M. Bernasconi, N. Nicoloso, and M. Parrinello, Phys. Rev. B **59**, 797 (1999).
[4] X. Zhao and D. Vanderbilt, Phys. Rev. B **65**, 075105 (2002).
[5] I. Clarke *et al.*, J. Bone Jt. Surg., Am. Vol. **85**, 73 (2003).
[6] L. Gremillard, J. Chevalier, T. Epicier, S. Deville, and G. Fantozzi, J. Eur. Ceram. Soc. **24**, 3483 (2004).
[7] D. Simeone, G. Baldinozzi, D. Gosset, M. Dutheil, A. Bulou, and T. Hansen, Phys. Rev. B **67**, 064111 (2003).
[8] T. Arima, S. Yamasaki, K. Yamahira, K. Idemitsu, Y. Inagaki, and C. Degueldre, J. Nucl. Mater. **352**, 309 (2006).
[9] J. M. Leger, P. E. Tomaszewski, A. Atouf, and A. S. Pereira, Phys. Rev. B **47**, 14075 (1993).
[10] O. Ohtaka, T. Yamanaka, S. Kume, N. Hara, H. Asana, and F. Izumi, Proc. Jpn. Acad., Ser. B: Phys. Biol. Sci. **66**, 193 (1990).
[11] J. Haines, J. M. Léger, and A. Atouf, J. Am. Ceram. Soc. **78**, 445 (1995).
[12] J. Haines, J. M. Léger, S. Hull, J. P. Petitet, A. S. Pereira, C. A. Perottoni, and J. A. H. da Jornada, J. Am. Ceram. Soc. **80**, 1910 (1997).
[13] H. Arashi, T. Yagi, S. Akimoto, and Y. Kudoh, Phys. Rev. B **41**, 4309 (1990).
[14] O. Ohtaka, T. Yamanaka, and T. Yagi, Phys. Rev. B **49**, 9295 (1994).
[15] H. M. Kandil, D. Greiner, and J. F. Smith, J. Am. Ceram. Soc. **67**, 341 (1984).
[16] E. H. Kisi and C. J. Howard, J. Am. Ceram. Soc. **81**, 1682 (1998).
[17] S. Chan, Y. Fang, M. H. Grinsditch, Z. Li, M. V. Nevitt, W. M. Robertson, and E. S. Zouboulis, J. Am. Ceram. Soc. **74**, 1742 (1991).
[18] B. L. Henke, E. M. Gullikson, and J. C. Davis, At. Data Nucl.

Data Tables **54**, 181 (1993).
[19] A. P. Mirgorodsky and P. E. Quintard, J. Am. Ceram. Soc. **82**, 3121 (1999).
[20] A. P. Mirgorodsky, M. B. Smirnov, and P. E. Quintard, Phys. Rev. B **55**, 19 (1997).
[21] S. Fabris, A. T. Paxton, and M. W. Finnis, Phys. Rev. B **61**, 6617 (2000).
[22] R. Devanathan, W. J. Weber, S. C. Singhal, and J. D. Gale, Solid State Ionics **177**, 1251 (2006).
[23] H. J. F. Jansen, Phys. Rev. B **43**, 7267 (1991).
[24] R. Orlando, C. Pisani, C. Roetti, and E. Stefanovich, Phys. Rev. B **45**, 592 (1992).
[25] R. H. French, S. J. Glass, F. S. Ohuchi, Y. N. Xu, and W. Y. Ching, Phys. Rev. B **49**, 5133 (1994).
[26] G. Jomard, T. Petit, A. Pasturel, L. Magaud, G. Kresse, and J. Hafner, Phys. Rev. B **59**, 4044 (1999).
[27] J. E. Lowther, J. K. Dewhurst, J. M. Léger, and J. Haines, Phys. Rev. B **60**, 14485 (1999).
[28] J. K. Dewhurst and J. E. Lowther, Phys. Rev. B **57**, 741 (1998).
[29] L. K. Dash, N. Vast, P. Baranek, M.-C. Cheynet, and L. Reining, Phys. Rev. B **70**, 245116 (2004).
[30] J. E. Jaffe, R. A. Bachorz, and M. Gutowski, Phys. Rev. B **72**, 144107 (2005).
[31] M. Sternik and K. Parlinski, J. Chem. Phys. **122**, 064707 (2005).
[32] D. R. Hamann, X. Wu, K. M. Rabe, and D. Vanderbilt, Phys. Rev. B **71**, 035117 (2005).
[33] *Physics Meets Mineralogy: Condensed-Matter Physics in Geosciences*, edited by H. Aoki, Y. Syono, and R. J. Hemley (Cambridge University Press, New York, 2000).
[34] B. B. Karki, L. Stixrude, and R. M. Wenzcovitch, Rev. Geophys. **39**, 507 (2001).
[35] P. Ravindran, L. Fast, P. A. Korzhavyi, B. Johansson, J. Wills, and O. Eriksson, J. Appl. Phys. **84**, 4891 (1998).
[36] Y. Le Page and P. Saxe, Phys. Rev. B **63**, 174103 (2001).
[37] Y. Le Page and P. Saxe, Phys. Rev. B **65**, 104104 (2002).
[38] *CRC Handbook of Chemistry and Physics*, 87th ed. (CRC, Boca Raton, FL, 2006).
[39] N. Schoeni and G. Chapuis, CRYSTALOGRAPH, available at http://escher.epfl.ch/crystalOgraph
[40] G. V. Lewis and C. R. A. Catlow, J. Phys. C **18**, 1149 (1985).
[41] S. E. Redfern, R. W. Grimes, and R. D. Rawlings, J. Mater. Chem. **11**, 449 (2001).
[42] J. M. Delaye and D. Ghaleb, Phys. Rev. B **61**, 14481 (2000).
[43] L. Cormier, D. Ghaleb, J. M. Delaye, and G. Calas, Phys. Rev. B **61**, 14495 (2000).
[44] J. D. Gale and A. L. Rohl, Mol. Simul. **29**, 291 (2003).
[45] R. E. Cohen, M. J. Mehl, and L. L. Boyer, Physica B **152**, 1 (1988).
[46] S. M. Ho, Mater. Sci. Eng. **54**, 23 (1982).
[47] The ABINIT code is a common project of the Université Catholique de Louvain, Corning Incorporated, and other contributors. See http://www.abinit.org.
[48] X. Gonze *et al.*, Comput. Mater. Sci. **25**, 478 (2002).
[49] X. Gonze *et al.*, Z. Kristallogr. **220**, 558 (2005).
[50] J. P. Perdew, K. Burke, and M. Ernzerhof, Phys. Rev. Lett. **77**, 3865 (1996).
[51] S. G. Louie, S. Froyen, and M. L. Cohen, Phys. Rev. B **26**, 1738 (1982).
[52] M. Rohlfing, P. Krüger, and J. Pollmann, Phys. Rev. Lett. **75**, 3489 (1995).
[53] B. Králik, E. K. Chang, and S. G. Louie, Phys. Rev. B **57**, 7027 (1998).
[54] D. Vanderbilt, Phys. Rev. B **41**, 7892 (1990).
[55] P. E. Blöchl, Phys. Rev. B **50**, 17953 (1994).
[56] N. A. W. Holzwarth, G. E. Matthews, R. B. Dunning, A. R. Tackett, and Y. Zeng, Phys. Rev. B **55**, 2005 (1997).
[57] N. A. W. Holzwarth, G. E. Matthews, A. R. Tackett, and R. B. Dunning, Phys. Rev. B **57**, 11827 (1998).
[58] G. Kresse and D. Joubert, Phys. Rev. B **59**, 1758 (1999).
[59] D. Vanderbilt, USPP, available at http://www.physics.rutgers.edu/dhv/uspp/
[60] M. Torrent and F. Jollet, USPP2ABINIT, available at http://www.abinit.org/PAW/USpp2Abinit-Manual-html/USppPAW.htm.
[61] Y. Wang and J. P. Perdew, Phys. Rev. B **44**, 13298 (1991).
[62] QUANTUM ESPRESSO is a community project for high-quality quantum-simulation software, based on density-functional theory, and coordinated by P. Giannozzi. See http://www.quantum-espresso.org and http://www.pwscf.org
[63] QUANTUM-ESPRESSO pseudopotentials are available at http://www.quantum-espresso.org/pseudo.php
[64] A. M. Rappe, K. M. Rabe, E. Kaxiras, and J. D. Joannopoulos, Phys. Rev. B **41**, 1227 (1990).
[65] J. Bennett and A. M. Rappe, OPIUM, available at http://lorax.chem.upenn.edu/Research/psp_gga.html
[66] M. Fuchs and M. Scheffler, Comput. Phys. Commun. **119**, 67 (1999).
[67] H. J. Monkhorst and J. D. Pack, Phys. Rev. B **13**, 5188 (1976).
[68] A. Kuwabara, T. Tohei, T. Yamamoto, and I. Tanaka, Phys. Rev. B **71**, 064301 (2005).
[69] J. K. Dewhurst and J. E. Lowther, Phys. Rev. B **57**, 741 (1998).
[70] S. Block, J. A. H. da Jornada, and G. J. Piermarini, J. Am. Ceram. Soc. **68**, 497 (1985).
[71] *Phase Diagrams for Zirconium and Zirconia Systems*, edited by H. M. Ondik and H. F. McMurdie (National Institute of Standards and Technology/American Ceramic Society, Columbus, Ohio, 1998).
[72] P. Bouvier, E. Djurado, G. Lucazeau, and T. Le Bihan, Phys. Rev. B **62**, 8731 (2000).
[73] S. K. Chan, private communication, reported in Kisi and Howard, J. Am. Ceram. Soc., **81**, 1682 (1998).
[74] Y. Kudoh, H. Takeda, and H. Arashi, Phys. Chem. Miner. **13**, 233 (1986).
[75] J. D. McCullough and K. N. Trueblood, Acta Crystallogr. **12**, 507 (1959).
[76] C. J. Howard, ; quoted in Mirgorodsky and Quintard, J. Am. Ceram. Soc. **82**, 3121 (1999).
[77] S. Kawasaki and T. Yamanaka, J. Mater. Sci. Lett. **13**, 514 (1994).
[78] N. M. Balzaretti and J. A. H. da Jornada, Phys. Rev. B **52**, 9266 (1995).
[79] M. V. Nevitt, S. Chan, J. Z. Liu, M. H. Grinsditch, and Y. Fang, Physica B **152**, 231 (1988).
[80] A. S. Pereira (private communication).
[81] C. J. Howard, R. J. Hill, and B. E. Reichert, Acta Crystallogr., Sect. B: Struct. Sci. **B44**, 116 (1988).
[82] *International Tables for Crystallography*, edited by T. Hahn (Springer-Verlag, Berlin, New York, Heidelberg, 2005), Vol. A.
[83] J. Cai and E. Anastassakis, Phys. Rev. B **51**, 6821 (1995).
[84] I. L. Chistyi, I. L. Fabelinskii, V. F. Kitaeva, V. V. Osiko, Y. V.

Pisarevskii, I. M. Sil'vestrova, and N. N. Sobolev, J. Raman Spectrosc. **6**, 183 (1977).
[85] K. Negita, Acta Metall. **37**, 313 (1989).
[86] R. N. Patil and E. C. Subbarao, J. Appl. Crystallogr. **2**, 281 (1969).
[87] R. N. Patil and E. C. Subbarao, Acta Crystallogr., Sect. A: Cryst. Phys., Diffr., Theor. Gen. Crystallogr. **A26**, 535 (1970).
[88] E. C. Subbarao, H. S. Maiti, and K. K. Srivastava, Phys. Status Solidi A **21**, 9 (1974).
[89] R. C. Garvie and S. Chan, Physica B **152**, 203 (1988).
[90] F. Frey, H. Boysen, and T. Vogt, Acta Crystallogr., Sect. B: Struct. Sci. **B46**, 724 (1990).
[91] G. R. Hugo and B. C. Muddle, Mater. Sci. Forum **56-58**, 357 (1990).
[92] H. Boysen, F. Frey, and T. Vogt, Acta Crystallogr., Sect. B: Struct. Sci. **B47**, 881 (1991).
[93] N. K. Simha, J. Mech. Phys. Solids **45**, 261 (1997).
[94] W. Zhou, H. Wu, and T. Yildirim, Phys. Rev. B **76**, 184113 (2007).
[95] D. K. Smith and H. W. Newkirk, Acta Crystallogr. **18**, 983 (1965).
[96] R. G. Wyckoff, *Crystal Structures*, 2nd ed. (Wiley, New York, 1963).
[97] V. V. Brazhkin, arXiv:cond-mat/0605626 (unpublished).
[98] S. Desgreniers and K. Lagarec, Phys. Rev. B **59**, 8467 (1999).
[99] C.-Z. Fan, S.-Y. Zeng, L.-X. Li, Z.-J. Zhan, R.-P. Liu, W.-K. Wang, P. Zhang, and Y.-G. Yao, Phys. Rev. B **74**, 125118 (2006).
[100] J. E. Lowther, J. K. Dewhurst, J. M. Léger, and J. Haines, Phys. Rev. B **60**, 14485 (1999).